Integration of bending operation in hybrid additive manufacturing chains based on powder bed fusion

Valentino Cristino[1*], *Rui* Sampaio[2], *João* Pragana[2], *Ivo* Bragança[3], *Carlos* Silva[2], *Paulo* Martins[2]

[1]Department of Electromechanical Engineering, University of Macau, Avenida da Universidade, Taipa, Macao, China
[2]IDMEC, Instituto Superior Tecnico, Universidade de Lisboa, Av. Rovisco Pais, 1049-001 Lisboa, Portugal
[3]CIMOSM, Instituto Superior de Engenharia de Lisboa, Instituto Politécnico de Lisboa, Portugal

Abstract. The concept of integration of conventional manufacturing technologies with metal additive manufacturing, namely metal forming, has gained interest within the research community and the industry due to its potential to overcome the limitations of long build times and reduced build volumes of laser powder fusion, expanding their applicability by making use of the advantages of each approach. This study focuses on the optimization of the production sequence of additively manufactured slender three-dimensional custom parts with specific angles by hybridization of metal additive manufacturing with bending. The methodology is based on experimental data obtained from the mechanical and formability characterization of the material through uniaxial tension and three-point bending tests, conducted in both its as-built and heat-treated conditions. This is complemented by finite element analysis of bending stages applied to a slender, three-dimensional, double U-shaped part. The study compares and analyses its fabrication using conventional laser powder bed fusion and hybrid additive manufacturing with bending. Results indicated that the understanding of the formability limits of the material and the use of finite element analysis in the part design for hybrid additive manufacturing can improve significantly the overall effectiveness of the process in terms of material saving, fabrication time and geometric tolerances.

Keywords: Hybrid additive manufacturing; Laser powder bed fusion; Bending; Formability.

1 Introduction

Laser powder bed fusion (LPBF) is a laser-based metal additive manufacturing (MAM) process that allows fabricating complex three-dimensional objects from a layer wise deposition process: a thin layer of powder is spread onto the building platform and a high-power laser melts the powder according to a predefined two-dimensional scanning path. The cycle repeats until the desired geometry is completed [1].

Although LPBF is capable of fabricating quality parts with high dimensional accuracy, superior mechanical properties, and complex geometry for a wide range of metals, the process is still somehow constrained by its limited build volume and recurrent defects like porosities, incomplete fusion holes, cracks, and impurities. Additionally, post-processing operations are often needed to remove support structures, obtain the required tolerances and finishing, and compensate for the distortions arising from thermal residual stresses of the heating- cooling cycles during material deposition.

One possible solution to overcome the above limitations is to integrate LPBF, concurrently or sequentially, with other traditional manufacturing processes [2]. One of the most common practices is post-processing with metal cutting processes, not only to remove the parts from the substrate, but also to improve the parts' geometric precision and surface quality [3]. However, integrating MAM with metal cutting during material deposition [4] is time-consuming, especially for large parts, and most times impractical due to limited accessibility within LPBF machines. The subsequent processing of the deposited material with processes such as incremental forming [5], forging [6] and sheet-bulk forming [7] was recently explored by different authors showcasing the potential of combining MAM with metal forming to produce preforms and near-net-shape parts in small to medium batch sizes.

Fig. 1 shows a schematic representation of two possible routes based on metal additive manufacturing route to fabricate a slender, three-dimensional S-shaped part, with the traditional MAM route consisting in LPBF and post-processing with metal cutting operations, while the alternative hybrid AM route resulting combines metal additive manufacturing with bending focusing in faster and fewer post-processing operations.

Research studies on the inclusion of bending operations with AM started with the study of Li and Rapthadu [8] and Papke et al. [9] on the bending commercial rolled sheets with additively manufactured elements. Huber et al. [10] studied the influence of the laser scanning parameters on the joint quality of AM deposited elements on commercial Ti6Al4V sheets.

* Corresponding author: vcristino@um.edu.mo

Previous work of Rosenthal et al. on the forming properties of additively manufactured nickel-based superalloy (Hastelloy X) [11] and AISI 316L [12] semi-finished sheets with different internal structures. Their studies showed that the deposited Hastelloy X semi-finished sheets have highly anisotropic behaviour, which is the result of material deposition, and subsequent heat treatment can approximate the material behaviour to that of commercial hot-rolled sheets used in traditional manufacturing processes. Moreover, the utilization of a hybrid AM route can increase the overall efficiency by at least 40% up to 680% when compared to conventional AM [12].

However, despite the potential of hybridizing LPBF with bending claimed in the above publications, studies continue to highlight the persistent difficulties related to the formability problems of deposited materials[13], limiting the applicability of the hybridization of LPBF with bending to low levels of plastic deformation, underscoring the need for further research in this area.

Under these circumstances, this work focuses on understanding the feasibility of hybridizing LPBF with bending operations (bottom side of Fig. 1). The workplan covers mechanical and formability tests of the deposited material in as-built and post-treated conditions, with the in-plane strains during tests measured through digital image correlation (DIC). Results are then used to design and fabricate a three-dimensional double U-shaped slender part, and the effectiveness of the overall methodology and hybridization of LBPF with bending is compared with conventional AM with LPBF.

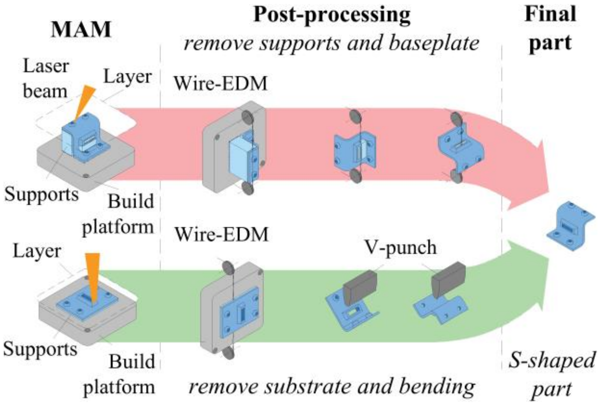

Fig. 1. Schematic representation of two manufacturing routes to fabricate a three-dimensional slender S-shaped part: (Top) Metal additive manufacturing (MAM) consisting of LPBF, and (bottom) hybrid metal additive manufacturing combining LPBF with bending.

2 Methods and procedures

2.1 Laser Powder Bed Fusion

Gas-atomized AlSi10Mg aluminium alloy powder supplied by SLM solutions® was used for this work. The Hitachi S-3400N, Type I scanning electron microscopy (SEM) was used to analyse the composition and measure the diameter of the AlSi10Mg powder, which ranges from 26 to 63 μm (Table 1).

Table 1. Chemical composition of the AlSi10Mg aluminium alloy powder used in LPBF.

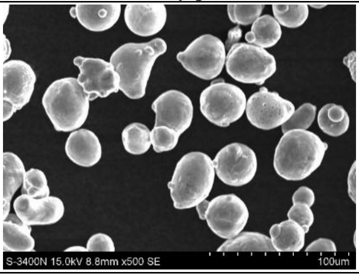

Element	wt.%
Al	Bal.
Si	10
Mg	0.4
Fe	0.13
Zn	0.01
Ti	0.01
Cu	0.01
Mn	0.01

A SLM 280HL 2.0 system equipped with a 400W laser was used to fabricate the different types of specimens used for this study. The build process was based on the optimized parameters provided by the equipment supplier, the oxygen content of the build chamber was kept under 0.1% with nitrogen, and the temperature of the build platform was set to 150ºC throughout layer-by-layer construction. All specimens were built horizontally to reduce the thermal gradients between the top and bottom layers. Table 2 summarizes the build parameters used in the deposition of the specimens.

The different specimens were removed from the substrate using a wire electrical discharge machining (wire-EDM). The specimens were tested in two different conditions: as-built and heat treated by annealing at 320ºC for three hours, followed by cooling inside the furnace. A minimum of 3 specimens for each test type and treatment condition was considered for testing.

Table 2. Main deposition parameters used in the fabrication of the three different specimens using LPBF.

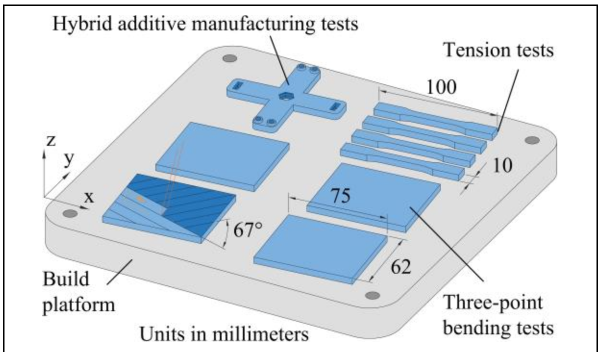

Laser power	370 W	Hatch spacing	0.15 mm
Spot size	0.06 mm	Scan pattern	Stripe
Scanning speed	1.335 m/s	Strip length	10 mm
Layer thickness	0.03 mm	Scan rotation	67º

2.2 Mechanical and formability tests

Tension and three-point bending tests were carried out with specimens milled to a constant thickness for 3 mm and according to the ASTM E8/E8M-16 and ASTM E290–14 standards.

The tension tests (Fig. 2a) were carried out in an INSTRON 5900 universal testing machine, and the three-point bend tests were (Fig. 2b) performed in an INSTRON SATEC 1200kN with the assistance of a multidirectional toolset to convert the vertical stroke into a horizontal movement using a cam slide unit consisting of a cylindrical punch moving against two cylindrical support fixtures placed at a distance apart and holding the specimens in place [14].

The evolution of the in-plane strains ε_1 and ε_2 during the tests were measured with a commercial digital image correlation (DIC) system with two 6-megapixel resolution cameras equipped with 50.2 mm focal length lenses and f/8 aperture from Dantec Dynamics (model Q-400 3D). The images were captured at a shutter frequency of 20 Hz and analysed with the INSTRA 4D software from Dantec Dynamics.

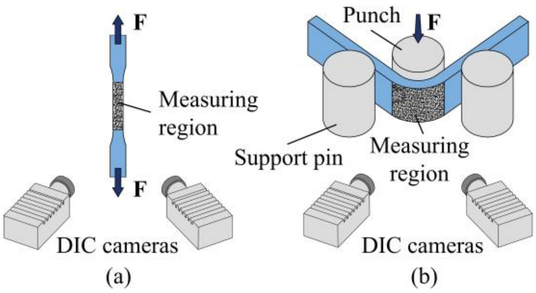

Fig. 2. Schematic representations of the (a) tension and (b) three-point bending tests.

2.3 Hybrid additive manufacturing test

The hybrid additive manufacturing tests is based on material deposition using LPBF of a flat cross-shaped preform followed by bending operations to obtain a three-dimensional double U-shaped slender part. The geometry of the cross-shaped preform along with details of the punch and die tool set used in the bending operations are presented in Fig. 3.

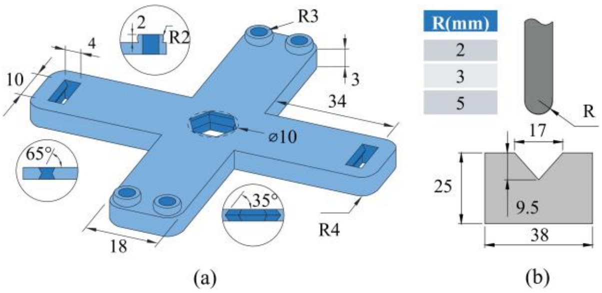

Fig. 3. (a) Geometry of the flat cross-shaped specimens and final three-dimensional double U-shaped parts. (b) Schematic representation of the punch and die tool set used in the bending operations.

For these tests, the specimens were directly removed from the substrate by wire-EDM and subjected to heat treatment by annealing, in order to reduce the number of post-processing operations (refer to Fig. 1). They were additionally used to provide a comparative analysis on the material usage, fabrication time, surface finish and geometric precision against a double U-shaped slender part built entirely by LPBF, following the process parameters previously shown in Table 2. This part was then removed from the substrate with wire-EDM and manually post-processed to remove the supports.

2.4 Finite Element Analysis

The in-house finite element computer program i-form 3D [15] was used to design and analyse the bending operations on the cross-shaped specimens. The program was built upon a modified weak form of Markov's rate of energy variational statement to include contact and sliding with friction between the specimens and the punches and die of the tool set,

$$\int_V \sigma'_{ij}\delta D_{ij}dV + \int_V \sigma_m \delta D_v dV - \int_{S_t} t_i\,\delta u_i dS + \int_{S_f}\left(\int_0^{|u_r|} \tau_f \delta u_r\right) dS = 0 \quad (1)$$

Equation (1) adopts a control volume V approach incorporating a 'updated Eulerian approach' with velocities u_i as the primary unknowns [16]. The first term of the expression involves the deviatoric Cauchy stress σ'_{ij} and the rate of deformation D_{ij} (viscous effects). The second term uses the hydrostatic stress σ_m and the volumetric rate of deformation D_v, analogous to hydrostatic effects on a viscous fluid. The incompressibility condition of the velocity field $D_v = 0$ is relaxed using a penalty function K, where $\sigma_m = (K/2)D_v$. The third and fourth terms in (1) refer to the tractions t_i applied on the boundary S_t of the control volume, and to the friction shear stress τ_f and the relative sliding velocity u_r acting on the contact interfaces S_f between the specimens and the punches and dies. Friction between the tool and the specimens was modelled with the law of constant friction, $\tau_f = mk$, where k represents the shear flow stress and m denotes the friction factor, considered as 0.1.

The material of the specimen was considered isotropic, following the Levy-Mises constitutive equations, with its flow stress and mechanical parameters to be presented in section 3.1. The specimens were discretized with meshes consisting of approximately 7500 hexahedral elements and the bending tools were discretized with contact-friction spatial triangles, with symmetry conditions along the yz plane (Fig. 4b). The average computation time for an Intel® Core™ i7-6950X with a CPU of 3.00GHz was of 45 minutes.

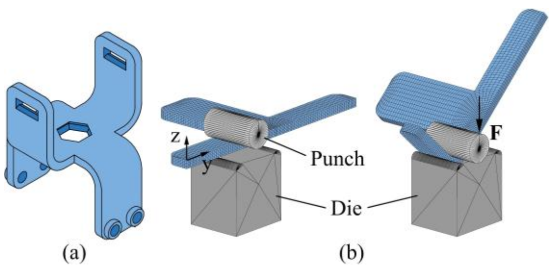

Fig. 4. (a) Geometry of the three-dimensional double U-shaped slender part used for this study and the finite element modelling (half-section) of a flat cross-shaped specimen at the (b) beginning and (c) end of bending.

3 Results and discussion

3.1 Mechanical and formability characterization

The flow curves of the as-built and annealed AlSi10Mg aluminium deposited by LPBF are shown in

Fig. 5a and their mechanical properties listed in Table 3. It can be observed that the as-built aluminium alloy presents higher strength and lower elongation at fracture than that of the annealed aluminium. The improvements on the formability of the annealed aluminium alloy can be observed in Fig. 5b, with its in-plane strain values at fracture much higher than the as-built aluminium alloy (refer to the X-markers in the second quadrant).

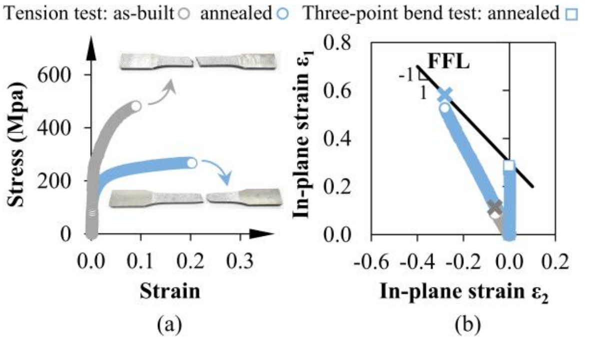

Fig. 5. Mechanical and formability characterization of the as-built and annealed AlSi10Mg aluminium deposited by LPBF: (a) Flow curves from tension tests and (b) Strain loading paths from tension and three-point bending tests.

Table 3. Summary of the mechanical properties of the aluminium alloy deposited by LPBF in the as-built and annealed conditions.

Testing condition	Young Modulus (GPa)	Yield strength (MPa)	Tensile strength (MPa)	Elongation at break (%)
As-built	52.4	262.9	440.9	9.4
Annealed	69.0	133.5	227.6	26.9

Because of the reduced ductility of the as-built aluminium alloy when subjected to tension tests, three-point bending results shown in Fig. 5b refer only to the annealed condition. The fracture forming limit (FFL) of the material (plotted as a solid black line) was predicted by passing a line with the theoretical slope '-1' [17] based on the average values of the in-plane strain at fracture resulting from the tension tests because no cracks were observed during the three point bending tests.

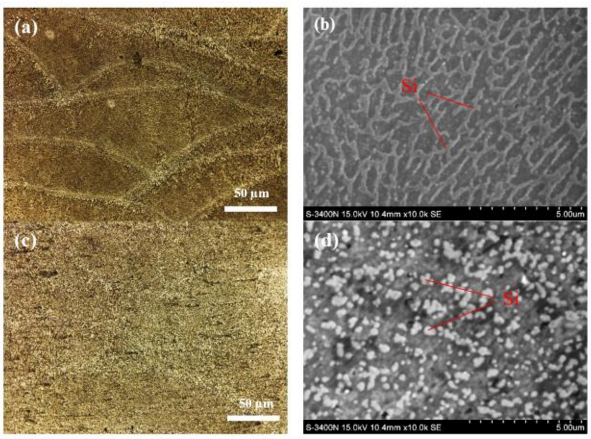

Fig. 6. Microstructure observations of metallurgical samples extracted from aluminium alloy specimens in its as-built state (a, b) and (c, d) after annealing.

The differences observed in the mechanical and formability limits can be attributed microstructure of the material (Fig. 6). It can be observed that individual melt pools with borders consisting of fine dendrite structures are clearly present along the as-built aluminium alloy, which is the result of rapid solidification rates, and the reheating effects result of the layer-by-layer deposition typical of LPBF [18].

A more detailed observation with SEM showed that the Si particles within the material are arranged in a dendritic structure (Fig. 6b). Meanwhile, the microstructure of the specimens after annealing (Fig. 6d) reveals that the boundaries of the melt pools had completely disappeared. In the as-built state of the aluminium alloy, these boundaries were present but later broke down into small particles, as seen in Fig. 6d.

3.2 Hybrid additively manufactured double U-shaped slender part

The methodology to design double U-shaped slender part by hybrid manufacturing with material deposition by LPBF and bending has its design, geometry and dimensions of the punch radii for the bending operation determined from the finite element and formability analysis. The slender part was designed with features to illustrate the potential improvements of hybridization of AM with bending over conventional AM: the bending angle was set to bending 90º, which maximizes the height of the part, and unique details like slots with inclined surfaces that can be only fabricated by AM allows to showcase the importance of part positioning and the requirement of support during LPBF.

Fig. 7 shows the finite element computed distribution of accumulated damage D^{Mc} using the McClintock ductile fracture criterion [19] for the two different punch radii at the end of a bending operation from a flat preform.

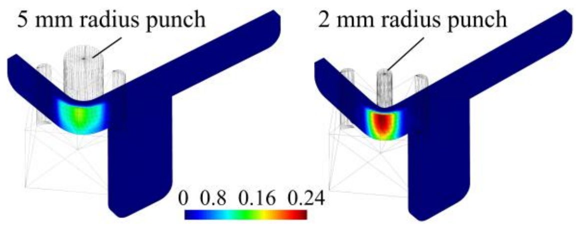

Fig. 7. Finite element distribution of damage according to the McClintock ductile damage criterion at the end of the first bending operation and using different punches.

The accumulated damage D^{Mc} is determined by,

$$D^{\mathrm{Mc}} = \int_0^{\bar{\varepsilon}} \eta \, d\bar{\varepsilon} \tag{2}$$

where $\bar{\varepsilon}$ is the effective strain, and $\eta = \sigma_m / \bar{\sigma}$ is the stress triaxiality accounted for crack opening by tension (mode I of fracture mechanics), which is the most likely mode of failure in the outer radius of the parts subjected to tensile stresses [17].

Results shown in Fig. 7 indicate that a punch radius of 2 mm radius increases the damage value, leading to strain values beyond the fracture forming limit of the material. This is evidenced in Fig. 8, coupled with photographs of the cracked bent region using different punch radius with the fracture faces perpendicular to direction of the applied tensile stress.

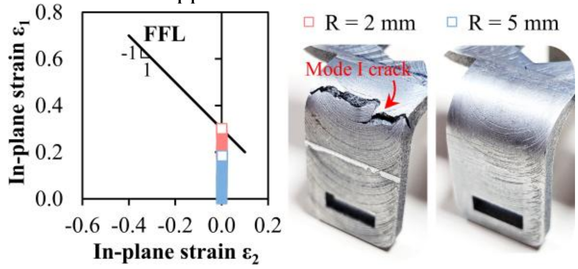

Fig. 8. Finite element strain loading paths along the outer radius during bending of flat plates into a three-dimensional double U-shaped slender part. Photographs are included for each case.

The material usage and waste, deposition time, geometric precision and surface details of the three-dimensional double U-shaped slender part using both fabrication routes of only additive manufacturing hybrid manufacturing by combining LBPF with bending are presented in Table 4.

The results showed that the hybrid AM route presents an improvement of 87.9% in material savings and an 85.7% reduction in the overall built time over the conventional AM route, as the post processing bending operations are carried out almost instantaneously. The hybrid AM route requires a minimum material for support (approximately 59% from conventional AM), only for the subsequent removal of the part from the substrate plate with wire-EDM. The removal of the supports on the part fabricated by conventional AM requires the use of small size grinding tools and other hand tools, which are time consuming and give rise to a non-uniform surface finishing. Regarding geometric tolerances, after the removal of the supports, a maximum deviation of 2.0º was found in the bent regions of the parts, mainly due to the thermal stresses that were generated during LPBF. In contrast, the part obtained from the hybrid AM route showed little to none geometric deviation, demonstrating that bending stages can also be used as post-processing calibration.

4 Conclusions

This study highlights the importance of understanding the formability limits of the material and the use of finite element analysis in part design for the hybridization of MAM with bending. This approach results in better material savings, reduced fabrication time, and tighter tolerances for the production of slender parts. The following conclusions can be drawn:

- The hybrid manufacturing route, combining LPBF and bending, significantly improves material savings and build time. Additionally, the bending operation can serve as a calibration step for the part's geometry.
- Formability test results indicate that material obtained directly from LPBF requires heat treatment to enhance its ductility.
- Finite element analysis has proven to be a valuable tool for designing slender components in hybrid additive manufacturing with bending. Its predictions of damage, using the McClintock ductile fracture criterion, show good agreement with both fracture forming limits obtained from tension and three-point bending, as well as with experimental bending operations.

Table 4. Comparison of the conventional and hybrid additive manufacturing routes for the fabrication of the case study with a double U-shaped slender part.

Manufacturing route	Powder volume	Support material volume	Build time	Final part
Conventional AM	541.2 cm^3	6.5 cm^3	8h58m	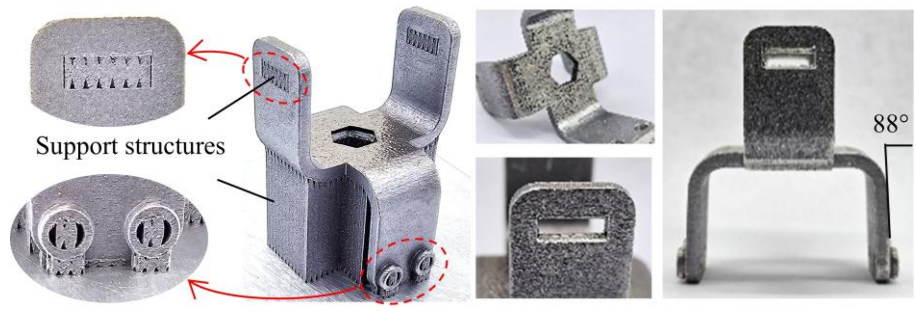
Hybrid AM	65.1 cm^3	2.7 cm^3	1h17m	

Acknowledgments

Valentino Cristino would like to acknowledge the support provided by the Multi-Year Research Grant (MYRG) of University of Macau (grant no. MYRG-GRG2024-00201-FST-UMDF).

References

1. Chowdhury, N. Yadaiah, C. Prakash, S. Ramakrishna, S. Dixit, L.R. Gupta, D. Buddhi, J. Mater. Res. Technol. **20**, 2109 (2022).
2. J.P.M. Pragana, R.F.V. Sampaio, I.M.F. Bragança, C.M.A. Silva, P.A.F. Martins, Adv. Ind. Manuf. Eng. **2**, 100032 (2021).
3. G. Manogharan, R.A. Wysk, O.L.A. Harrysson, Int. J. Comput. Integr. Manuf. **29**, 473 (2016).
4. X. Luo and M.C. Frank, Rapid Prototyp. J. **16**, 100 (2010).
5. G. Ambrogio, F. Gagliardi, M. Muzzupappa, L. Filice, J. Manuf. Process. **37**, 386 (2019).
6. F. Meiners, J. Ihne, P. Jürgens, S. Hemes, M. Mathes, I. Sizova, M. Bambach, R. Hama-Saleh, A. Weisheit, Procedia Manuf. **47**, 261 (2020).
7. M. Merklein, R. Schulte, T. Papke, J. Mater. Process. Technol. **291**, 117032 (2021).
8. Y. Li R. Rapthadu, in Vol. 1 Process. (American Society of Mechanical Engineers, 2017).
9. T. Papke, P. Dubjella, L. Butzhammer, F. Huber, O. Petrunenko, D. Klose, M. Schmidt, M. Merklein, Procedia CIRP **74**, 290 (2018).
10. F. Huber, T. Papke, M. Kerkien, F. Tost, G. Geyer, M. Merklein, M. Schmidt, J. Laser Appl. **31**, (2019).
11. S. Rosenthal, S. Platt, R. Hölker-Jäger, S. Gies, S. Kleszczynski, A.E. Tekkaya, G. Witt, Mater. Sci. Eng. A **753**, 300 (2019).
12. S. Rosenthal, M. Hahn, A.E. Tekkaya, S. Platt, S. Kleszczynski, G. Witt, Int. J. Precis. Eng. Manuf. Technol. **9**, 1021 (2022).
13. C. López, A. Elías-Zúñiga, I. Jiménez, O. Martínez-Romero, H. R. Siller, J.M. Diabb, Materials (Basel). **11**, 2542 (2018).
14. M.S.T. Sapage, J.P.M. Pragana, R.F.V. Sampaio, I.M.F. Bragança, C.M.A. Silva, P.A.F. Martins, J. Adv. Join. Process. **9**, 100175 (2024).
15. C. V. Nielsen, P.A.F. Martins, Metal Forming (Elsevier, 2021).
16. D. Banabic, in Sheet Metal Forming Processes (Springer, Berlin, Heidelberg, 2010).
17. P.A.F. Martins, N. Bay, A.E. Tekkaya, A.G. Atkins, Int. J. Mech. Sci. **83**, 112 (2014).
18. L. Thijs, K. Kempen, J.-P. Kruth, J. Van Humbeeck, Acta Mater. **61**, 1809 (2013).
19. F.A. McClintock, J. Appl. Mech. **35**, 363 (1968).